Chemistry SELECT

www.chemistryselect.org

A journal of

ChemPubSoc Europe

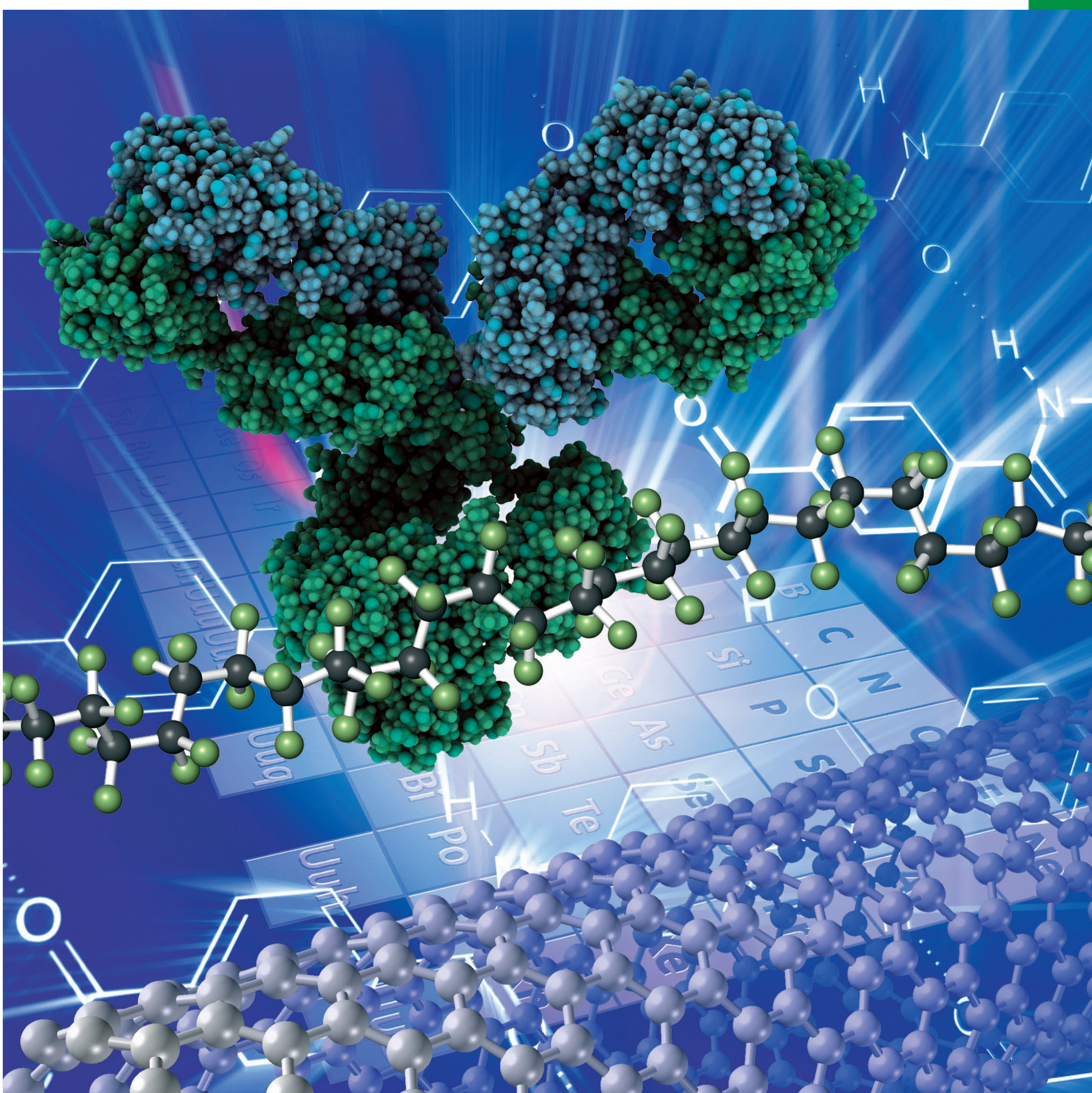

REPRINT

WILEY-VCH

Inorganic Chemistry

Facile Fabrication of Fe_3O_4@poly(acrylic) Acid Based Ferrofluid with Magnetic Resonance Imaging Contrast Effect

The Tam Le,[a] Hoa Du Nguyen,[a] Thi Ngoc Linh Nguyen,[b] Thi Hong Tuyet Phan,[a] Dinh Quang Ho,[a] Thien Vuong Nguyen,[c, g] Mrs. Thi Thu Hiep Le,[a] Thi Kim Oanh Vuong,[d, g] Khoa Hai Le,[c] Duc Duong La,*[e, f] Trong Lu Le,[c, g] and Lam Dai Tran[c, g]

Magnetic resonance imaging (MRI) has emerged as one of the most promising techniques, which employs nanoscience and imaging technology, for early diagnosis of the cancers. In this work, magnetic nanoparticles of Fe_3O_4@ poly(acrylic) acid (PAA) were synthesized using a low cost thermal decomposition method from iron ions precursor and utilized as a signal agent for MRI imaging. The Fe_3O_4 magnetic nanoparticles obtained from $FeCl_2.4H_2O$ precursor at the reaction temperature of 315 °C in 1-octadcene solvent are of spherical shape with average diameter of 8.4 nm and high saturation magnetization (M_s) of 60.05 emu/g. After phase transferred with PAA, the magnetic Fe_3O_4@PAA fluid is highly stable in a wide range of pHs solution (5 - 9) and wide range of NaCl concentrations (50 - 300 mM) with zeta potential of −35.7 mV. The prepared Fe_3O_4@PAA fluid showed noncytotoxicity to the Hep-G2, MCF-7, RD cancer cell line and Vero healthy cell line. MRI *in-vitro* results showed that transverse relaxation rate r_2 was around 158.4 $mM^{-1}s^{-1}$ and the signal intensity was not affected by the pHs solution and NaCl concentrations. *In-vivo* test on rabbit revealed the clear observation of rabbit's body parts after injection of the Fe_3O_4@PAA magnetic fluid with retention time of 90 minutes in the body.

1. Introduction

Nanomaterials have been extensively studied for the biomedical application such as magnetic hyperthermia, targeted therapy, targeted drug delivery, computed tomography (CT) and magnetic resonance imaging (MRI).[1–8] Together with the computed tomography, magnetic resonance imaging (MRI) is considered as one of the useful techniques for research, clinical diagnosis, treatment of patients owing to high quality of tissue imaging.[9–12] The quality of magnetic resonance image is not only dependent on the equipment and imaging technology, but also strongly dependent on the contrast agents, which is used to enhance the contrast of the selected zones in the body with the surrounding tissues. Contract agents could reduce relaxation allowances T_1, T_2, or both T_1 and T_2, as characteristic parameters for two relaxation processes of protons.[13,14] T_1 paramagnetic contrast agents are often based on dysprosium (Dy^{3+}), gadolinium (Gd^{3+}) derivatives or manganese (Mn^{2+}). In which, gadolinium (Gd^{3+}) derivatives including acid gadobenic, gadobutrol, gadodiamid, gadofosveset, acid gadopentetic, acid gadoteric, gadoteridol, gadoversetamid and acid gadoxetic have been widely used in the MRI contrast agents for many commercial products.[15–18] However, these contrast agents have certain limits such as short circulation time with long scanning time, and high toxicity to the kidney, liver, lung and heart of human.[19–21] Thus, it is necessary to develop safe and effective contrast agents for the magnatic resonance imaging in practical application.

Magnetic Fe_3O_4 nanoparticles are one of the most promising materials used for the enhancement of MRI contrast image due to its high magnetic saturation and superparamagnetic properties.[14,22–24] Recent publised works showed that Fe_3O_4 nanopaticles could shorten T_2 transverse relaxation time, as a result, darken the tissues, which enhances the contrast in MRI imaging.[25–27] However, magnetic property of Fe_3O_4 nanoparticles depends significantly on particle sizes, thus the control of particle sizes plays an important role for incerase of relaxation parameters in MRI. It has been demonstrated that

[a] Dr. T. Tam Le, Prof. H. Du Nguyen, Prof. T. Hong Tuyet Phan, Dr. Dinh Quang Ho, M. Thi Thu Hiep Le
Vinh University, 182 Le Duan, Vinh City 460000, Vietnam
[b] Dr. T. Ngoc Linh Nguyen
Thai Nguyen University of Sciences, Tan Thinh Ward, Thai Nguyen City 250000, Vietnam
[c] Dr. T. Vuong Nguyen, Mr. K. Hai Le, Dr. T. Lu Le, Prof. L. Dai Tran
Institute for Tropical Technology, Vietnam Academy of Science and Technology, 18 Hoang Quoc Viet Road, Hanoi 100000, Vietnam
[d] Dr. T. Kim Oanh Vuong
Institute of Materials Science, Vietnam Academy of Science and Technology, 18 Hoang Quoc Viet Road, Hanoi 100000, Vietnam
[e] Dr. D. Duong La
Laboratory of Advanced Materials Chemistry, Advanced Institute of Materials Science, Ton Duc Thang University, Ho Chi Minh City, Vietnam
[f] Dr. D. Duong La
Faculty of Applied Sciences, Ton Duc Thang University, Ho Chi Minh City, Vietnam
E-mail: laducduong@tdtu.edu.vn
[g] Dr. T. Vuong Nguyen, Dr. T. Kim Oanh Vuong, Dr. T. Lu Le, Prof. L. Dai Tran
Graduate University of Science and Technology, Vietnam Academy of Science and Technology, 18 Hoang Quoc Viet Road, Hanoi 100000, Vietnam

Supporting information for this article is available on the WWW under https://doi.org/10.1002/slct.202003015

Fe_3O_4 with large nanoparticle sizes was unstable and short circulation time in the body.[28,29] On the other hand, the small Fe_3O_4 nanoparticles could enhance the biological compatibility, long remaining time in the body, which resulted in high quality of MRI image.[30–32]

The synthesis of size-controled and uniform Fe_3O_4 nanoparticles is difficult to achieve. Many approaches have been employed to produce the magnetic Fe_3O_4 nanoparticles such as co-precipitation, microware, hydrothermal, ultrasonic and microfluidic techniques.[28,33–36] However, majority of these methods utilized water as a reaction media, which resulted in large particle size, non-uniformity in shape. These disadvantage hindered the utilization of the magnetic nanomaterials in *in-vivo* biomedical applications. In order to obtain high quality magnetic nanoparticles for biomedical applications, thermal decomposition of organic ferro salt in high boiling-point organic solvent was used to obtain small magnetic nanoparticles with high crystallization, good dispersion, and high equivalent-grade.[37–41] However, the limit of this method is to use expensive organic precursors such as $Fe(acac)_3$ or $Fe(CO)_5$, oleyamin (OLA), oleic acid (OA) and 1,2-hexadecandiol.[37,38,40,42] Therefore, the selection of appropriate precursors and polymers with low cost to produce high quality Fe_3O_4 nanoparticles is always desirable and challenging.

Herein, we report the synthesis of magnetic nanoparticles by thermal decomposition method using ferrous (II) salt as precursor and 1-octadecene (OCD) and 1-octadecanol (OCD-ol), as solvent and accelerating agents, respectively. Effects of ferrous (II) salt precursors ($FeSO_4.7H_2O$ and $FeCl_2.4H_2O$) and reaction temperature on morphologies and the size of Fe_3O_4 particles are also investigated. The magnetic nanoparticles in solvent are then undergone a phase-transferred process with poly(acrylic) acid (PAA) ligand followed by surface functionalization with COOH group in order to form stable and homogeneous dispersion in water as ferrofluid.[43–45] This approach to fabricate Fe_3O_4 particles is considered to be environmental friendly and facile to scale up. The characterizations of the prepared materials such as morphology, crystallinity, magnetic properties as well as biological durability of magnetic fluid are invesitigated in detail. Moreover, *in-vitro* and *in-vivo* experiments are also carried out and discussed to evaluate toxicity of the nanoparticles.

2. Results and discussion

2.1. Characterization of Fe_3O_4 nanoparticles

Figure 1 shows the effect of precursors ($FeSO_4.7H_2O$ and $FeCl_2.4H_2O$) on the morphologies of the prepared Fe_3O_4 magnetic nanoparticles. When $FeSO_4.7H_2O$ was used, the obtained Fe_3O_4 magnetic nanoparticles with average size of around 7.1 ± 1.3 nm are in ununiform shape with unclear grain boundary (Figure 1a and 1b). When $FeCl_2.4H_2O$ was employed as precursor, magnetic nanoparticles are of spherical shape with monodispersion, clear grain boundary, and average size of 8.1 ± 0.8 nm (Figure 1c and d). This can be concluded that the Fe_3O_4 nanoparticles with uniform size distribution obtained by

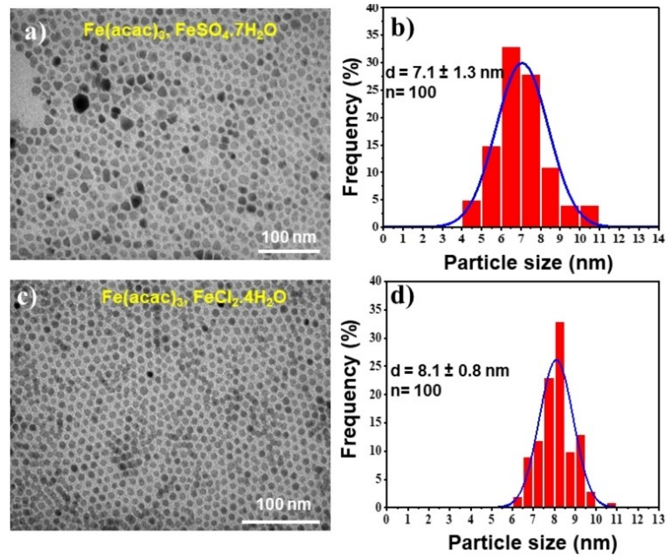

Figure 1. The typical TEM images and the corresponding size distribution histograms of the OA/OLA-coated Fe_3O_4 NPs synthesized with different inorganic iron (II) compounds: (a, b) $FeSO_4.7H_2O$; (c, d) $FeCl_2.4H_2O$ (Scale bar: 100 nm).

$FeCl_2.4H_2O$ precursor are more suitable for the MRI application than that of $FeSO_4.7H_2O$.

The effect of the temperature on the morphologies of the Fe_3O_4 obtained from $FeCl_2.4H_2O$ precursor is shown in Figure 2. It can be clearly seen that at the low temperature of 270 °C and 295 °C (Figure 2a and b), the resultant Fe_3O_4 nanoparticles are in unround and ununiform shape with average diameters of 5.5 ± 1.3 nm and 6.9 ± 0.8 nm, respectively. However, when reaction temperature increases to the 315 °C (Figure 2c), the uniform and spherical shape of Fe_3O_4 with 7.9 ± 0.5 nm in diameter are observed, which indicates that the reaction temperature has geat effect on the formation of the magnetic nanoparticle.[41,42]

The crystallinity of the Fe_3O_4 nanoparticles obtained from $FeCl_2.4H_2O$ precursor at temperature of 315 was analyzed by the X-ray diffraction pattern as shown in Figure 3a. It is obvious from the figure that the the XRD pattern of the Fe_3O_4 nanoparticles shows the characteristic peaks at 30.16°; 35.49°; 43.01°; 53.78°; 57.21° and 62.73°, which are attributed to the (220), (311), (400), (422), (511) and (440) planesof the Fe_3O_4, respectively. The Debye–Scherrer equation can be also employed to determine average crystal size:

$$d = \frac{K\lambda}{B\cos\theta} \tag{3}$$

where, K is a constant dependent on the crystallite shape, θ is the degree (position of the peak), λ is the X-ray wavelength, and B represents the full width at half maximum (FWHM) of the peak.

The HRTEM image and SAED results (Figure 2d and e) show the defined d distance between the crystal planes of materials

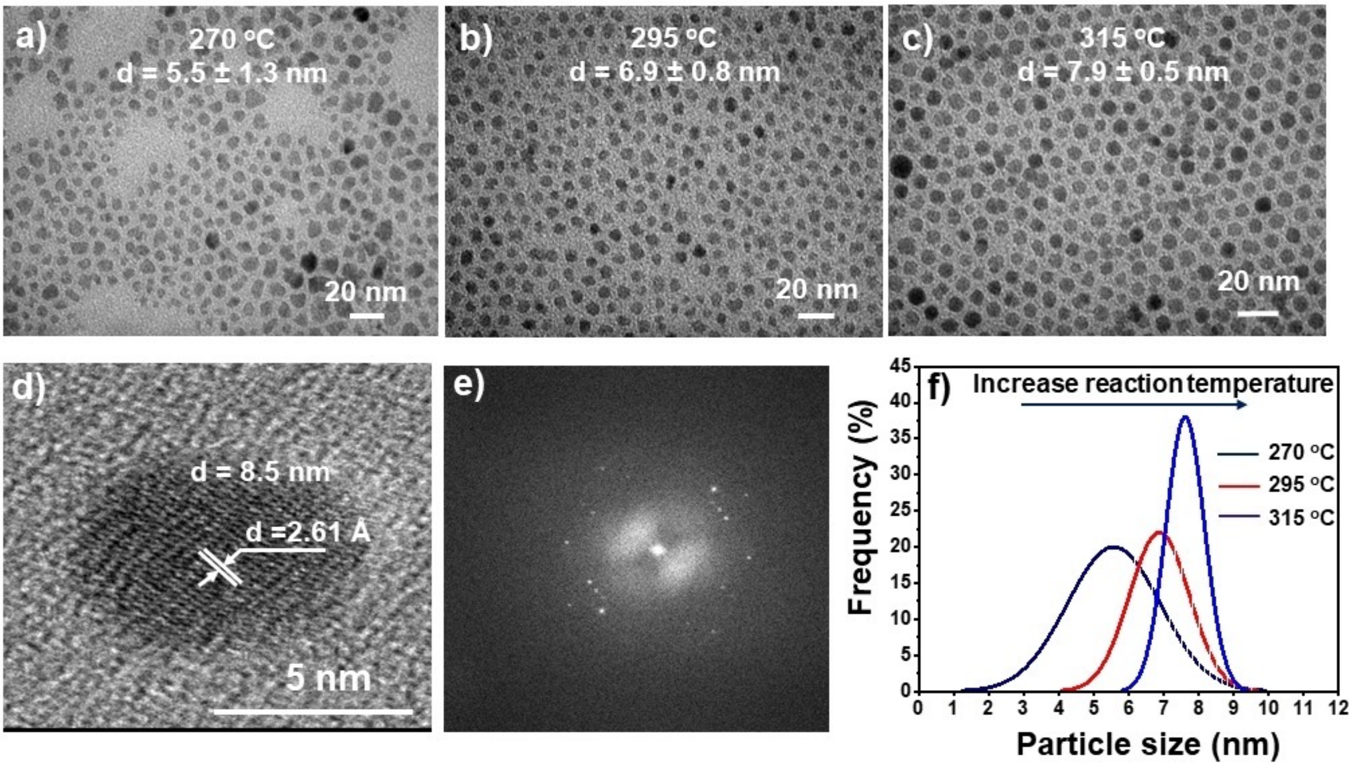

Figure 2. The TEM images (a–c), HRTEM images (d), SAED pattern (e) and their corresponding size distribution histograms (f) of the OA/OLA-coated Fe_3O_4 NPs prepared from different temperature.

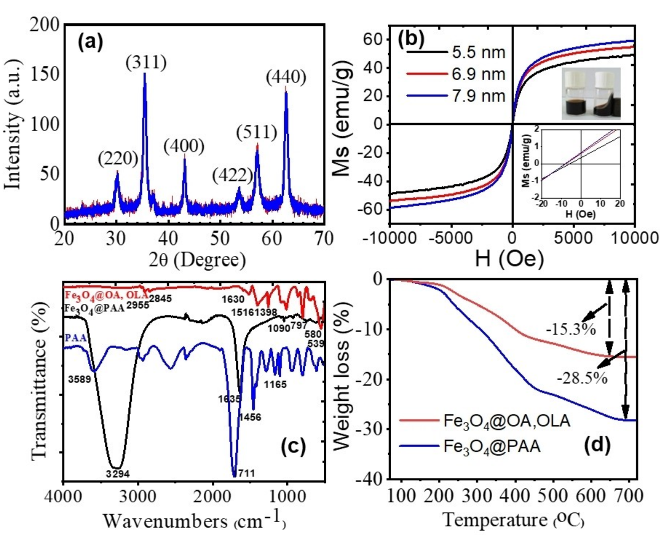

Figure 3. (a) XRD patterns (7.9 ± 0,5 nm); (b) Magnetization (H) curves of Fe_3O_4 nanoparticles (inset is the enlarged hysteresis loop at low magnetic field, the solid curves are the fitting curves calculated by using the Langevin function); (c) FT-IR spectra of Fe_3O_4@PAA, poly(acrylic acid) (PAA), Fe_3O_4@OA,OLA; and (d) TGA scans of OA/OLA and of Fe_3O_4@PAA NPs.

with the values of 2.61 A°, 3.01 A°, and 2.09 A°, which are attributed to (311), (220), and (400 planes of Fe_3O_4 nanocrystals), respectively.[47]

The average crystal size calculated from Debye–Scherrer equation is approximately 7.6 nm, which is consistent with particle size obtained from TEM study.

Magnetic property of Fe_3O_4 nanoparticles in the external magnetic fields from −10 kOe to 10 kOe, is presented in Figure 3b. It can be obvious that the Fe_3O_4 nanoparticles have a saturated magnetization value (M_s) of 49.80 emu/g, 55.37 emu/g and 60.05 emu/g corresponded to the particle sizes of 5.5 nm, 6.9 nm and 7.9 nm, respectively, at 300 K. The coercive fields value (Hc) of Fe_3O_4 with particle sizes of 5.5, 6.9, and 7.9 nm was calculated to be 6, 7.5, and 8 Oe, respectively. The remanence magnetizations (M_r) of Fe_3O_4 with various particle sizes of 5.5, 6.9, and 7.9 nm were also determined to be 0.35, 0.55, and 0.6 emu/g, respectively. This result confirms that the Fe_3O_4 nanoparticles is superparamagnetic. Futhermore, the saturated magnetic fields of the nanoparticles increase along with the increased sizes of the Fe_3O_4 nanoparticles. This high value of saturated magnetization of the Fe_3O_4 nanoparticles is desirable for the biomedical applications.

The chemical nature of surfactant/reductant OA, OLA and Fe_3O_4 nanoparticles is characterized by the FTIR spectra as shown in Figure 3c. It can be seen that absorption peak at 2955 cm^{-1} and 2845 cm^{-1} are vibrations of C–H groups in OA and OLA molecules. A weak stretching band at 1635 cm^{-1} is assigned to the deforming fluctuation of NH_2 complex of the OLA molecule. Two absorption peaks at 1516 cm^{-1} and 1398 cm^{-1} are ascribed to asymmetric and symmetric (COO^-)

group in the OA molecule. These results confirm that OA and OLA uniformly cover on the surface of Fe_3O_4 magnetic nanoparticles, which is consistent to the previous works.[48] Furthermore, the FTIR spectrum of Fe_3O_4@OA/OLA also appear strong absorption bands at 539 cm^{-1}, which is ascribed to Fe–O bonding in magnetic Fe_3O_4 nanoparticles. The IR spectrum of PAA shows two strong peak at 3589 cm^{-1} và 1711 cm^{-1}, which are assigned to the typical stretching vibrations of O–H and C=O of -COOH group. These bands shifted to 3294 cm^{-1} and 1635 cm^{-1}, respectively, in the IR spectrum of Fe_3O_4@PAA, which are dued to the interaction between PAA and the Fe_3O_4 nanoparticles.

Thermal properties of the Fe_3O_4@OA/OLA and Fe_3O_4@PAA samples were investigated using the TGA analysis as shown in Figure 3d. In the TGA spectrum of Fe_3O_4@OA/OLA, two typical steps of weight loss are observed. In first step, the samples loose about 3.15 % of weight at the temperature range of 50–250 °C, which can be assigned to organic solvents and/or moisture absorbed on the surface of the material. In second step, the weight loss of 12.15 % occurred at the temperature range of 250–650 °C, which is dued to the decomposition of OA/OLA molecules. Thus, it can be concluded that the remaining weight of around 85 % is the weight of the Fe_3O_4 nanoparticles and 15 % of weight accounted for the organic coating layer of OA/OLA. Similarly, the TGA thermal analysis diagram of Fe_3O_4@PAA samples shows the total weight loss of about 28.5 % in the temperature range from 90 to 650 °C, due to the losses of H_2O, OA, OLA and PAA (Figure 3d).

2.2. Particle size and Stability of the PAA-coated Fe_3O_4 nanoparticles

Since Fe_3O_4 @OA/OLA particles are difficult to disperse in the water, thus, modification of the Fe_3O_4@OA/OLA particles with functional groups such as PAA is necessary to enable the dispersability of the material in aqueous solution. TEM (Figure 4a) and HRTEM (Figure 4b) images indicate that Fe_3O_4@PAA magnetic nanoparticles are of spherical shape, uniform distribution with average size of 8.4 ± 1.2 nm (TEM). The zeta potential of Fe_3O_4@PAA magnetic nanoparticles was calculated to be −35.7 mV. The dynamic light scattering (DLS) diagram indicates that the particle sizes of obtained Fe_3O_4@PAA are in range has 10 to 80 nm, and most of the particles have particle size of 20 nm (Figure 4d). This result indicates that the obtained Fe_3O_4@PAA particles after coating and transferred phase with PAA are narrow, small distribution and relatively stable. Especially, after 6 months of storage, the magnetic fluid is still highly homogeneous with small change in zeta potential of −34.1 mV (Figure 4f) in comparison with the initial zeta potential of −35.7 mV.

2.3. In vitro cytotoxicity results

The cytotoxicity of Fe_3O_4@PAA samples was tested with Hep-G2, MCF-7, RD and Vero cell lines followed Sulforhodamine B (SRB) assay from previous work,[49] result is shown in Figure 5.

It can be obvious from the result that DMSO solvent do not cause toxicity on the cells as the cell viability still remains almost 100 % in the DMSO solvent. However, majority of Hep-

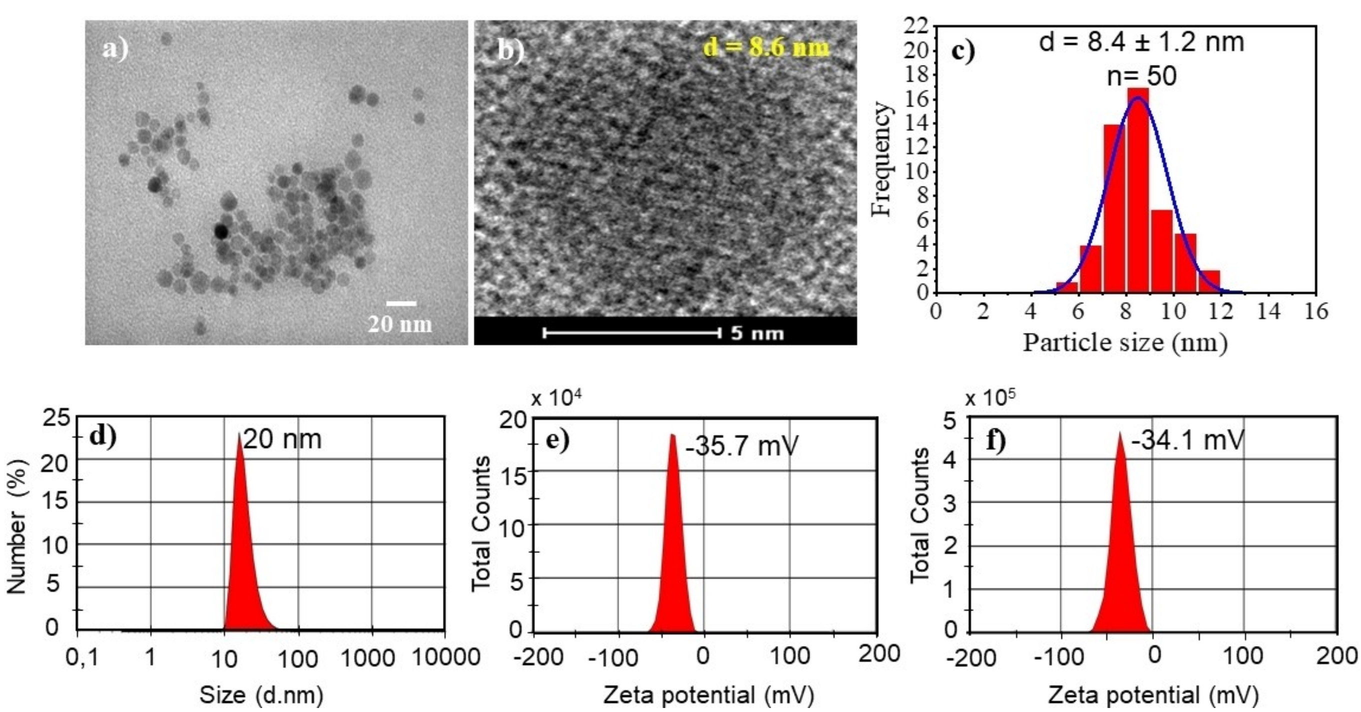

Figure 4. The typical TEM image (Scale bar: 20 nm) (a), HRTEM image (Scale bar: 5 nm), (c) the size distribution histograms of the PAA-coated Fe_3O_4 NPs, size distribution and Zeta potentials of the PAA-coated Fe_3O_4 NPs (d, e, and f).

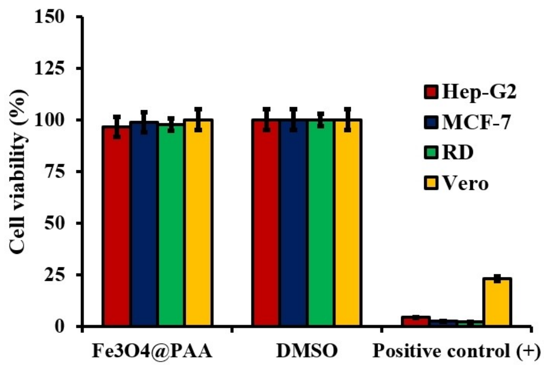

Figure 5. Effect of hollow Fe_3O_4 NPs on cellular proliferation and cellular morphology of Human hepatocellular carcinoma (Hep-G2), Human rhabdomyosarcoma (RD), Human breast adenocarcinoma (MCF-7) and Vero cells lines.

G2, MCF-7, RD cancer cells are killed after 72 hours of testing and causing a strong proliferation inhibition for Vero healthy cells in the positive control condition. In Fe_3O_4@PAA magnetic fluid, the cell viability was determined to be 96.56%, 98.75%, 97.65% and 100% for Hep-G2, MCF-7, RD, and Vero cells, respectively, which indicates that Fe_3O_4@PAA nanoparticles are negligible toxic to the cancer cell lines.[50] This result confirms that Fe_3O_4@PAA nanoparticles are safe to use for the bilogical application.

Figure 6 exhibits the morphologies of the cells in the presence of the Fe_3O_4@PAA fluid. It can be seen from the figure that the morphologies of the Hep-G2 cells and Vero cells in the presence of Fe_3O_4@PAA nanoparticles with concentrations of 25 μg/mL and 50 μg/mL are vertually unchanged in comparison with the controlled condition (Figure 6a and d). This further confirms that the Fe_3O_4@PAA nanoparticles do not cause toxicity to the cells. This is explained by a coating layer of the PAA on the surface of Fe_3O_4 nanoparticles.

2.4. Contrast enhancement in MRI

The superparamagnetic Fe_3O_4@PAA nanoparticles induce a decrease in transverse relaxation time T_2, leading to an increase in contrast of the MRI images. To evaluate the role of magnetic nanoparticles as a contrast agent, MRI imaging was carried out in defined protocol and in different concentrations of nanoparticles.

Figure 7 (a-e) presents T_2-weighted MR images of samples with the increase in the Fe_3O_4@PAA fluid concentrations with various values of TE. The considerable contrast can be clearly observed even at relatively small concentration. These results indicate that the transverse relaxation time T_2 decreases along with the increase of nanoparticles, as a result, enhancing the MR signal.

The choice of pulse sequence timing parameters determines the contrast in spin-echo images (SE). The TR value controls the amount of T_1 weighting, and the TE value controls the amount of T_2 weighting. The traditional model in SE imaging: Short TR/Short TE→T_1- weighted; Long TR/Short TE→PD- weighted; Long TR/Long TE→T_2- weighted; Short TR/Long TE→not used.

Another way to understand the effect of TE on T_2-weighting is to consider the signals generated by two tissues with different T_2 values. When TE is short, the echo occurs quickly before T_2-decay happened, hence the tissues are not differentiated. If TE is long, the relative differences in signal decay between the two tissues become more noticeable, and hence more "T_2-weighting".

With TE of 35 ms, signal intensity changes significantly compared to the sample at Fe_3O_4@PAA 0.01 mM concentration. In MRI imaging technology, TE of 50 ms value or higher are

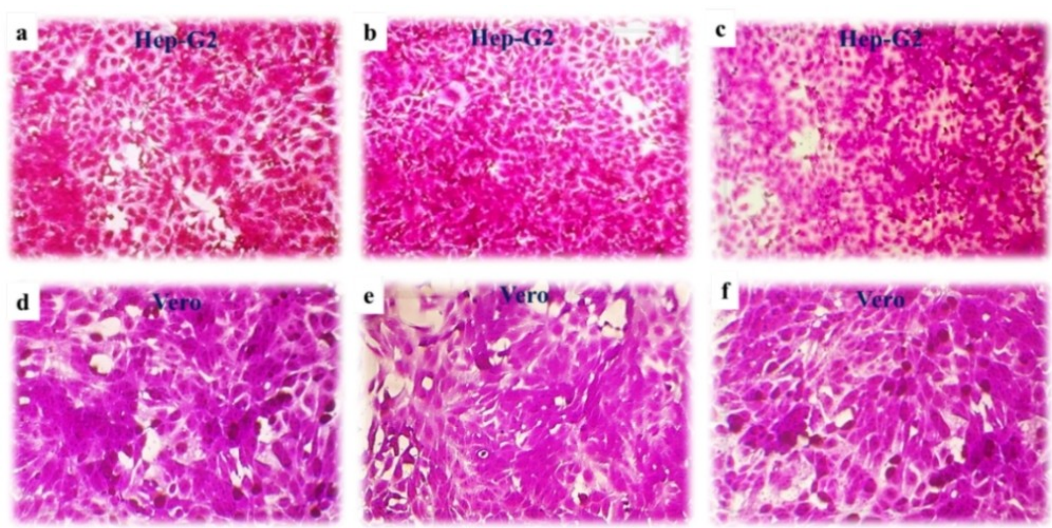

Figure 6. Optical images of Hep-G2 and Vero (e-f) cell lines before (a) and after addition of Fe_3O_4@PAA fluid with concentration of 25 μg/mL (b) and 50 μg/mL (c); and optical images of Vero cell line before (d) and after addition of Fe_3O_4@PAA fluid with concentration of 25 μg/mL (e) and 50 μg/mL (f).

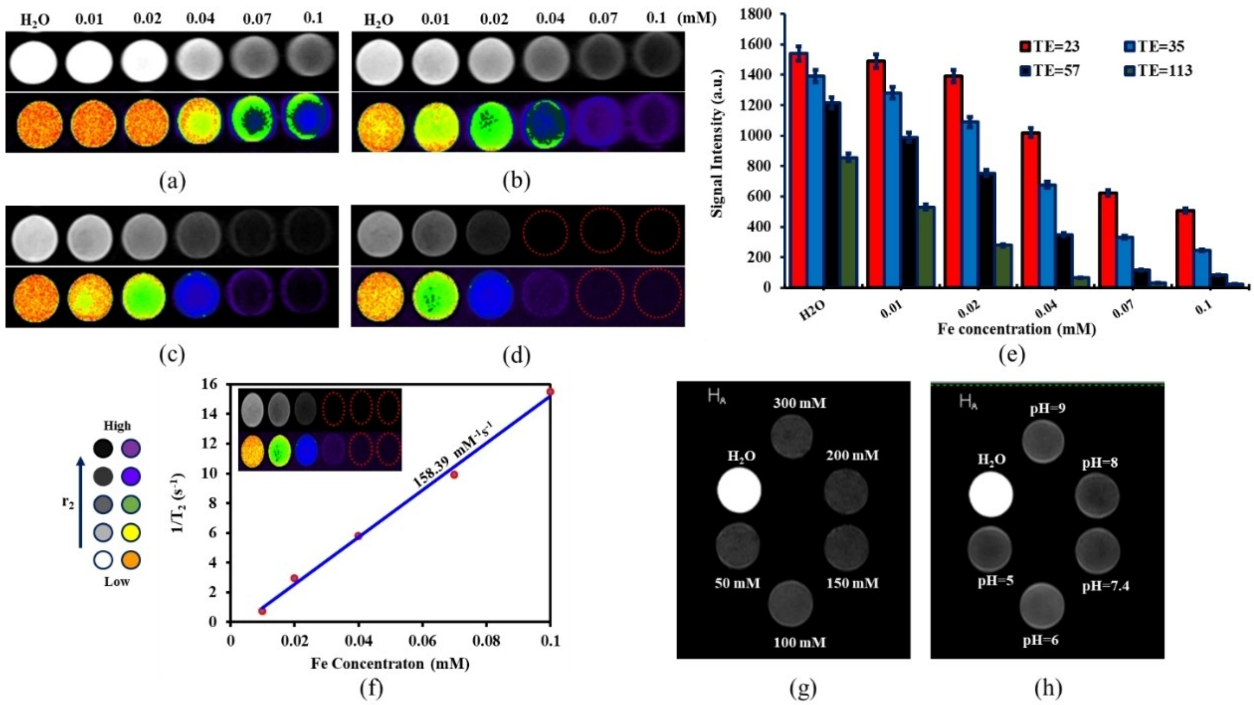

Figure 7. T_2 - weighted MRI of Fe_3O_4@PAA at different conditions, (a) TE = 23 ms; (b) TE = 35 ms; (c) TE = 57 ms; (d) TE = 113 ms, TR = 3500; (e) MRI signal intensity at the different concentrations of the MNPs and various values of TE; (f) $1/T_2$ (R_2) - Fe concentration plot of the Fe_3O_4@PAA nanoparticles at 1.5 T; and T_2-weighted MRI of Fe_3O_4@PAA at different NaCl concentrations (g) and at different pHs solution (h). The error bars represent the standard deviations.

often applied for MRI in accordance with T_2-weighted mode.[51,52] With smaller TE value, necessary time to collect signal will be shorted, which is suitable for the clinical applications.

In-vitro MRI images used Fe_3O_4@PAA magnetic fluid as contrast agents and transverse relaxation rate r_2 are presented in Figure 7f. The transverse relaxation rate r_2 of Fe_3O_4@PAA nanoparticles in the water was determined by taking the slope of $1/T_2$ linear matching compared to Fe concentration, found to be 158.4 ($mM^{-1}s^{-1}$). This r_2 value is higher than commercial products based on Fe_3O_4 such as Ferumoxide (Feridex), AMI-25 (Feridex; Endorem), SHU 555 C (Supravist) (Table 1) and in the publication of Ruitao Cha et al.[53] Transverse relaxation rate r_2 of Fe_3O_4@PAA nanoparticles is also higher than SHU-555 A (Ferucarbotran),[54,55] with hydrodynamic diameter of grain (58 nm) is three times larger than the size of Fe_3O_4@PAA (20 nm) particles. The high value r_2 of Fe_3O_4@PAA samples is ascribed to the high crystalization of materials, mono-dispersion, and uniform particles size.

It have been previous demonstrated that magnetic fluid was highly stable over a wide range of salt concentrations (from 50 to 300 mM), and pHs range (from 5 to 9).[46] The MRI image was taken in various salt concentrations of 50 mM, 100 mM, 150 mM, 200 mM, 300 mM. and various pHs solution of 5, 6, 7.4, 8, and 9. The results are shown in Figure 7g and 7 h. It can be clearly seen that the signal intensities are almost unchanged in salt solution and studied pH values. Considering to the physiological conditions in the human body with salt concentration of 165 mM and pH value of 7.4, Fe_3O_4@PAA magnetic fluid can be effectively used as a contrast agent in the body.

Figure 8a shows MR images of the liver, kidney of a rabbit: before (control) and after injection of ferrofluid Fe_3O_4@PAA into the ear vein for 10, 30, 60 and 90 minutes. The MRI results with Fe_3O_4@PAA contrast agents in T_2 weighted mode show that MRI images enhance in contrast by darkening the tissues and organs comapred to that of before the injection (negative contrast). After ferrofluid injected for 10 minutes, liver and kidney of rabbit are clearer than before injection. Signal intensity (SI) after injecting Fe_3O_4@PAA contrast substance is 730.1 with the liver tissue's area of 0.8 cm^2, which is 2.3 times higher than signal intensity in the same location before injection (314.7). After 60 minutes of injection, the kidney image is clearer than that of liver observation. However, after 90 minutes of injection, signal intensity of the liver tissues and kidney were significantly decreased. While T2 relaxation time defined in liver reduces from 240 ms down to 205 ms (liver) after 10 minutes, the T2 relaxation time in kidney was negligibly decreased from 230 ms down to 210 ms after 90 minutes of injecting time (Figure 8b).

Circulation time of Fe_3O_4@PAA fluid in the body was relatively long up to 90 minutes, which can be explained by the small, uniform in particle size and good biological compatibility. [59] The small size of particle enable the ease movement from reticule-endothelial system (RES) and endothelial phagocyte system which prolong the time to reach and accumulate in the tissues and tumors. On the other hand, the contrast substances with the larger sizes of from 50 to 100 nm

Table 1. Relaxation rate r_2 of Fe_3O_4@PAA and several commercial Fe_3O_4 nanoparticle-based MRI contrast agents.

Brand name	Ligand shell	Core size/ Hydrodynamic diameter (nm)	r_2 relaxation rate ($mM^{-1}s^{-1}$)	Target	Company/application/development-phase	Ref.
Ferumoxides (Feridex IV, Endorem), AMI-25	Dextran	5–6 80-150	100[1] 158[2]	Liver, spleen bone marrow	AMAG Pharmaceuticals Guerbet Approved[3]	[54]
Code 7228, Ferumoxy-toL, Feraheme, Rienso	Carboxymethyl-dextran	58	83[2]	MRA	AMAG Pharmaceuticals, Takeda Pharmaceut-ical Company Limited/approved for iron deficiency anemia[4]	[54,55]
CLIO-Tat	Dextran	5 30	62[2]	–	–	[14]
Sinerem, Combidex (AMI-227) Ferumoxtran-10	Dextran	4–6 20–40	78 [1] 87.6 [2]	MRA, liver, spleen, bone marrow	Guerbet AMAG Pharmaceuticals/phase III[5]	[54]
WSIO (MEIO)	DMSA	4 –	78[2]	–	–	[14]
WSIO (MEIO)	DMSA	6 –	106 [2]	–	–	[14]
WSIO (MEIO)	DMSA	9 –	130[2]	–	–	[14]
P904	Amino-alcohol-glucosederivative	4-6 21	87[2]	MRA, athero-sclerosi, adipos-ity	Guerbet/preclinical	[54]
VSOP–C184 Ferropharm	Citrate	4-5 7–9	29[1] 33.4[2]	MRA	Ferropharm GmbH/phase I	[54]
Au-Fe_3O_4	PEG	20 –	114[2]	–	–	[14]
Ferucarbotran (SHU-555 A), Resovist	Carboxydextran	4.2 50-100	151[1] 189[2]	Liver, spleen bone marrow	Bayer Healthcare Pharmaceuticals/approved[4] EU, Japan, USA	[54]
MION-46 L	Dextran	4–6 8–20	34.8[1]	MRA, lymph nodes, tumor, infarction	Center for Molecular Imaging Research, Char-lestown, MA/preclinical	[54]
SHU-555 C Ferucarbotra, Supravist	Carboxydextran	3–4 20-30	41[1] 38[2]	MRA, lymph nodes	Bayer Healthcare Pharmaceuticals/phase II [6]	[54]
$Al(OH)_3$, Fe_3O_4@PAA	Polyacrylic Acid and Aluminum Hydroxide	7 200–250	83.6[2]	–	–	[56]
C-USPION	Citrate	10–15 30	102[2]	–	–	[57]
D-SPIONs	Dextran	12 50	140.7	–	–	[58]
Fe_3O_4@PAA	Poly (acrylic acid)	6-8 20	158.4[2]	Current study	Current study	

Note. [1] Measured at 0.47 T, 37 °C. [2] Measured at 1.5 T, 37 °C. [3] No longer produced and distributed since 2011. [4] No longer distributed in Europe since 2009, only available in Japan (international pharmacy). [5] Application for clinical approval from EMEA withdawn in 2007. [6] No longer being developed.

are rapidly caught by macrophages of endothelial system and eliminated quickly in the liver, kidney before reaching to the tumors or targeted tissues.[30–32,60] This result shows that, Fe_3O_4@PAA contrast substances fabricated in this work are suitable to increase the contrast under T_2 shooting mode in MRI, which can diagnose exactly the cancer tissues.

3. Conclusions

In summary, Fe_3O_4 magnetic nanoparticles have been successfully synthesized by thermal decomposition method, using the inorganic precursor substances. The results show that Fe_3O_4 magnetic nanoparticles obtained from $FeCl_2.4H_2O$ precursor are in spherical shape and small particle size of 8.1 ± 0.8 nm with saturation magnetization value (M_s) of 60.05 emu/g, which is considered as a supermagnetic material. The Fe_3O_4@PAA magnetic nanoparticles showed highly stable in water with the average particle size of 8.4 nm and zeta potential of -35.7 mV. The Fe_3O_4@PAA magnetic fluid was nontoxic to Hep-G2, MCF-7, RD cancer cells in wide range of NaCl salt concentrations of 50–300 mM, and pHs range of 5–9. *In-vitro* MRI results showed the high value of transverse relaxation rate r_2 of 158.4 $mM^{-1}s^{-1}$ and were not affected by pH solution and NaCl salt concentration. *In-vivo* test in rabbit indicated that the picture of body parts was clearly observed after the injection of the Fe_3O_4@PAA fluid with T_2 weighted shooting mode with long circulation time of contrast agents in body up to 90 minutes. With these outstanding properties, Fe_3O_4@PAA magnetic fluid prepared from low cost of precursors is promising as a negative contrast agent for the MRI imaging technique in practical application.

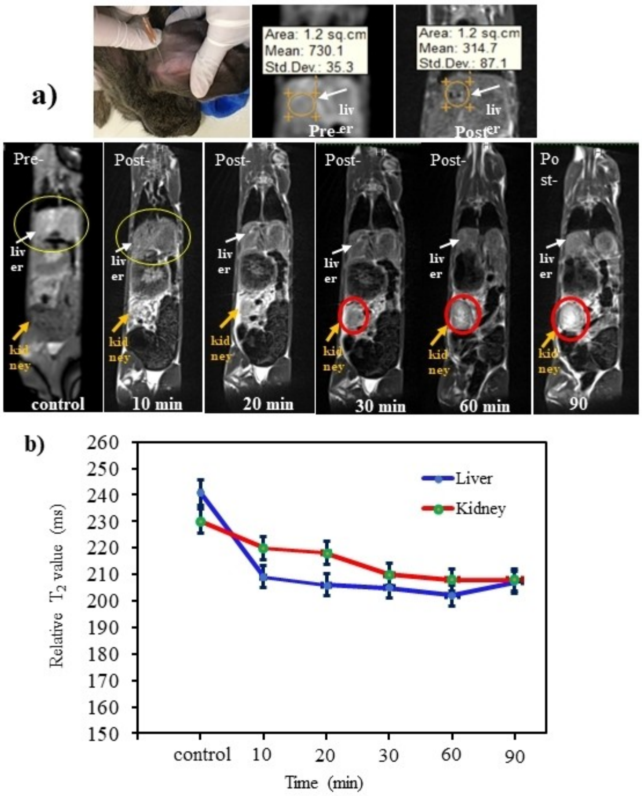

Figure 8. T2-weighted MR images of the liver, kidney of a rabbit: before (control) and after injection of ferrofluid Fe_3O_4@PAA into the ear vein for 10, 30, 60 and 90 minutes (a); (b) The corresponding relative T_2 values extracted from liver (orange circle) and kidney (red circle) sites.

Supporting Information Summary

The Supporting Information includes the detailed experimental section of this work.

Acknowledgements

This research was financially supported by the Ministry of Education and Training (MOET) under Project No. B2019-TDV-03 (L.T.T).

Conflict of Interest

The authors declare no conflict of interest.

Keywords: Magnetic resonance imaging (MRI) · magnetic properties · nanoparticles · poly(acrylic) acid · magnetic Fe_3O_4@PAA fluid

[1] R. Ranganathan, S. Madanmohan, A. Kesavan, G. Baskar, Y. R. Krishnamoorthy, R. Santosham, *Int. J. Nanomed.* **2012**, *7*, 1043–60.
[2] D. A. LaVan, T. McGuire, R. Langer, *Nat. Biotechnol.* **2003**, *21*, 1184–1191.
[3] A. Cavalcanti, B. Shirinzadeh, R. A. Freitas, T. Hogg, *Nanotechnology.* **2008**, *19*, 015103.
[4] V. Wagner, A. Dullaart, A. K. Bock, A. Zweck, *Nat. Biotechnol.* **2006**, *24*, 1211–1217.
[5] S. Y. Srinivasan, K. M. Paknikar, D. Bodas, V. Gajbhiye, *Nanomedicine.* **2018**, *13*, 1221–1238.
[6] L. S. Arias, J. P. Pessan, A. P. M. Vieira, T. M. T. D. Lima, A. C. B. Delbem, D. R. Monteiro, *Antibiotics.* **2018**, *7*, 1–32.
[7] M. E. F. Brollo, J. M. Orozco-Henao, R. López-Ruiz, D. Muraca, C. S. B. Dias, K. R. Pirota, M. Knobel, *J. Magn. Magn. Mater.* **2016**, *397*, 20–27.
[8] Z. Hedayatnasab, F. Abnisa, W. M. A. W. Daud, *Mater. Des.* **2017**, *123*, 174–196.
[9] B. Fischl, A. M. Dale, *PNAS.* **2000**, *20*, 11050–11055.
[10] N. Gogtay, J. N. Giedd, L. Lusk, K. M. Hayashi, D. Greenstein, A. C. Vaituzis, P. M. Thompson, *PNAS.* **2004**, *101*, 8174–8179.
[11] J. Xian, M. Chen, Z. Jin, *Chinese Medical Journal.* **2015**, *128*, 3–5.
[12] S. Kakeda, Y. Korogi, *Neuroradiology.* **2010**, *52*, 711–721.
[13] C. F. G. C. Geraldes, S. Laurent, *Contrast Media Mol. Imaging.* **2009**, ***4***, 1–23.
[14] B. Hyon, B. Na, I. C. Song, T. Hyeon, *Adv. Mater.* **2009**, *21*, 2133–2148.
[15] P. Caravan, J. J. Ellison, T. J. McMurry, R. B. Lauffer, *Chem. Rev.* **1999**, *99*, 2293–2352.
[16] D. H. Kim, S. H. Choi, S. Y. Kim, M. J. Kim, S. S. Lee, J. H. Byun, *Radiology.* **2019**, *291*, 651–657.
[17] P. Hermann, J. Kotek, V. Kubíček, I. Lukeš, *Dalt Trans.* **2008**, *9226*, 3027–47.
[18] L. Gao, J. Zhou, J. Yu, Q. Li, X. Liu, L. Sun, *Sci. Rep.* **2017**, *7*, 1–13.
[19] D. J. Todd, J. Kay, *Annu. Rev. Med.* **2016**, *67*, 273–291.
[20] P. Marckmann, L. Skov, K. Rossen, A. Dupont, M. B. Damholt, J. G. Heaf, *J. Am. Soc. Nephrol.* **2006**, *17*, 2359–2362.
[21] European Medicines Agency, *Assessment report.* **2017**, *EMA/411650*, 1–82.
[22] R. Weissleder, D. D. Stark, B. L. Engelstad, B. R. Bacon, C. C. Compton, D. L. White, *Am. J. Roentgenol.* **1989**, *152*, 167–173.
[23] Y. Xiang, J. Wang, *Quant Imaging Med Surg.* **2011**, *1*, 35–44.
[24] P. Reimer, T. Balzer, *Eur Radiol.* **2003**, *13*, 1266–1276.
[25] M. W. Marashdeh, B. Ababneh, O. M. Lemine, A. Alsadig, K. Omri, L. E. Mir, *Results Phys.* **2019**, *15*, 102651, 1–5.
[26] L. T. Tam, N. H. Du, N. T. N. Linh, N. T. Vuong, P. T. H. Tuyet, N. T. H. Hoa, N. Q. Thang, H. T. Ha, T. D. Chien, B. L. Minh, L. T. Lu, L. D. Duong, S. V. Bhosale, T. D. Lam, *J. Nanosci. Nanotechnol.* **2020**, *20*, 5338–5348.
[27] P. M. Khaniabadi, D. Shahbazi-gahrouei, M. S. Jaafar, A. M. S. A. Majid, S. Shahbazi-gahrouei, *Avicenna J Med Biotech.* **2017**, *9*, 181–188.
[28] S. Ahmadi, C. H. Chia, S. Zakaria, K. Saeedfar, N. Asim, *J. Magn. Magn. Mater.* **2012**, *324*, 4147–4150.
[29] S. I. El-Dek, M. A. Ali, S. M. El-Zanaty, S. E. Ahmed, *J. Magn. Magn. Mater.* **2018**, *458*, 147–155.
[30] C. Bai, P. Hu, N. Liu, G. Feng, D. Liu, Y. Chen, Y. Zhang, *ACS Nano* **2020**, 1–26.
[31] Q. Wang, M. Shen, T. Zhao, Y. Xu, J. Lin, Y. Duan, *Sci. Rep.* **2015**, ***5***, 1–8.
[32] G. Wang, X. Zhang, A. Skallberg, Y. Liu, Z. Hu, X. Mei, *Nanoscale.* **2014**, *6*, 2953–2963.
[33] S. Majidi, F. Z. Sehrig, S. M. Farkhani, M. S. Goloujeh, A. Akbarzadeh, Artif Cells, *Nanomedicine Biotechnol.* **2016**, *44*, 722–734.
[34] Y. X. Chen, S. P. Chen, Z. Y. Zhou, N. Tian, Y. X. Jiang, S. G. Sun, *J. Am. Chem. Soc.* **2009**, *131*, 10860–10862.
[35] V. T. Thu, A. N. Mai, L. T. Tam, H. V. Trung, P. T. Thu, B. Q. Tien, T. D. Lam, *J. Electron. Mater.* **2016**, *45*, 2576–2581.
[36] L. T. Tam, N. H. Du, T. D. Lam, P. T. H. Tuyet, L. T. Nhan, *Vietnam J Sci Technol.* **2018**, *54*, 341–347.
[37] S. Sun, H. Zeng, *J. Am. Chem. Soc.* **2002**, *124*, 8204–8205.
[38] S. Sun, H. Zeng, D. B. Robinson, S. Raoux, P. M. Rice, S. X. Wang, *J. Am. Chem. Soc.* **2004**, *4*, 126–132.
[39] J. Park, K. An, Y. Hwang, J. Park, H. Noh, J. Kim, T. Hyeon, *Nat. Mater.* **2004**, *3*, 891–895.
[40] V. T. K. Oanh, L. T. Tam, D. H. Doan, N. X. Truong, N. X. Ca, V. T. Thu, L. T. Lu, T. D. Lam, *Mater. Chem. Phys.* **2020**, *245*, 1–22.
[41] V. T. K. Oanh, T. D. Lam, L. T. Lu, P. D. Viet, P. H. Nam, N. T. H. Le, *Mater. Chem. Phys.* **2015**, *163*, 537–544.
[42] L. T. Lu, N. T. Dung, L. D. Tung, C. T. Thanh, O. K. Quy, N. V. Chuc, S. Meanosono, N. T. K. Thanh, *Nanoscale.* **2015**, *7*, 19596–19610.
[43] A. W. Dunn, S. M. Ehsan, D. Mast, G. M. Pauletti, H. Xu, J. Zhang, *Mater. Sci. Eng. C* **2015**, *46*, 97–102.
[44] W. Wang, L. Zheng, F. Lu, R. Hong, M. Z. Q. Chen, L. Zhuang, *AIP Adv.* **2017**, *7*, 1–8.

[45] Y. Y. Xu, M. Zhou, H. J. Geng, J. J. Hao, Q. Q. Ou, S. D. Qi, *Appl. Surf. Sci.* **2012**, *258*, 897–902.
[46] V. T. K. Oanh, T. D. Lam, V. T. Thu, L. T. Lu, P. H. Nam, L. T. Tam, D. H. Manh, N. X. Phuc, *J. Electron. Mater.* **2016**, *45*, 4010–4017.
[47] S. J. Iyengar, M. Joy, C. K. Ghosh, S. Dey, R. K. Kotnala, S. Ghosh Magnetic, *RSC Adv.* **2014**, *4*, 64919–64929.
[48] N. Wu, L. Fu, M. Su, M. Aslam, K. C. Wong, V. P. Dravid, *Nano Lett.* **2004**, *4*, 383–386.
[49] P. Skehan, R. Storeng, D. Scudiero, A. Monks, J. McMahon, D. Vistica, *J. Natl. Cancer Inst.* **1990**, *82*, 377–387.
[50] C. Tao, Y. Chen, D. Wang, Y. Cai, Q. Zheng, L. An, *Nanomaterials.* **2019**, *9*, 1–13.
[51] W. R. Nitz, P. Reimer, *Eur. Radiol.* **1999**, *1046*, 1032–1046.
[52] B. Plewes, *Imaing&Therapetic Technology.* **1994**, *14*, 1389–1404.
[53] R. Cha, J. Li, Y. Liu, Y. Zhang, Q. Xie, M. Zhang, *Colloids Surfaces B Biointerfaces.* **2017**, *158*, 213–221.
[54] H. Ittrich, K. Peldschus, N. Raabe, M. Kaul, G. Adam, *Fortschr Rontgenstr.* **2013**, *185*, 1149–1166.
[55] G. B. Toth, C. G. Varallyay, A. Horvath, M. R. Bashir, P. L. Choyke, H. E. Daldrup-Link, *CKidney Int.* **2017**, *92*, 47–66.
[56] Manuel Antonio González-Gómez, Sarah Belderbos, Susana Yañez-Vilar, Yolanda Piñeiro, Frederik Cleeren, Guy Bormans, Christophe M. Deroose, Willy Gsell, Uwe Himmelreich, José Rivas, *Nanomaterials.* **2019**, *9*, 1–20.
[57] Ariya Saraswathy, Shaiju S. Nazeer, Madhumol Jeevan, Nirmala Nimi, Sabareeswaran Arumugam, Vijayakumar S. Harikrishnan, P. R. Harikrishna Varma, Ramapurath S. Jayasree, *Colloids Surfaces B Biointerfaces.* **2014**, *117*, 216–224.
[58] Ariya Saraswathy, Shaiju S. Nazeer, Nirmala Nimi, Sabareeswaran Arumugam, Sachin J. Shenoy, Ramapurath, S. Jayasr, *Carbohydr. Polym.* **2014**, **101**, 760–768.
[59] Y. Feng, Y. Zong, T. Ke, E. Jeong, D. L. Parker, Z. Lu, *Pharm. Res.* **2006**, *23*, 1736–1742.
[60] H. Daldrup-Link, G. Simon, R. Brasch, K. Turetschek, E. Kaindl, T. M. Link, E. J. Rummeny, *Radiology.* **2006**, *12*, 2661–2672.

Submitted: August 3, 2020
Accepted: October 29, 2020